A GENUINELY MULTIDISCIPLINARY JOURNAL

CHEMPLUSCHEM

CENTERING ON CHEMISTRY

Accepted Article

Title: Oxazolium iodide modified perovskites for solar cell fabrication

Authors: Manuel Salado, Erfan Shirzadi, Samrana Kazim, Fei Zhaofu, M K Nazeeruddin, Paul J Dyson, and Shahzada Ahmad

To be cited as: *ChemPlusChem* 10.1002/cplu.201700471

Link to VoR: http://dx.doi.org/10.1002/cplu.201700471

A Journal of ChemPubSoc Europe

WILEY-VCH

www.chempluschem.org

Oxazolium iodide modified perovskites for solar cell fabrication

Manuel Salado,[a] Erfan Shirzadi,[c,d] Samrana Kazim,[a] Zhaofu Fei,[d] Mohammad Khaja Nazeeruddin,[c] Paul J. Dyson[d], Shahzada Ahmad*[a,b]

Abstract: Perovskites solar cells are gaining interest due to their attractive solar-to-electricity conversion efficiencies, although they suffer from certain problems, such as sub-optimal ion migration and stability issues. We studied the inclusion of a phenyloxazolium salt (2-phenyl-3-methyl-oxazolium iodide) in methyl ammonium lead triiodide ($MAPbI_3$) based perovskite solar cells. The fabricated solar cells not only gave improved photovoltaic properties, but importantly the oxazolium cation can protect the perovskite layers from UV exposure as it down-converts electromagnetic irradiation, i.e. the photons are absorbed in UV and re-emitted at a different wavelength. The loading of 2-phenyl-3-methyloxazolium iodide in the perovskite precursor solution was optimized, the resulting perovskite films characterized, and the solar cells fabricated from them evaluated for their performance. Overall, this simple approach facilitates the optimization of the performance parameters of perovskites films for solar cell applications.

Introduction

Perovskite solar cells (PSCs) are foreseen as an attractive candidate for electricity generation form solar energy. The remarkable photovoltaic properties of perovskites are due to their high absorption coefficient, high carrier mobility, long diffusion length and direct band gap material properties, together with flexibility of architects and charge selective contact.[1,2] However, the long-term stability[3], hysteresis behavior[4–6] and an understanding of the working principles[7] are still not fully resolved. Recently, attempts to understand the fundamental working principle and mechanism of PSCs have been reported, especially the current-voltage (*J-V*) hysteresis behavior.[8,9]

Recent results points towards the likelihood that multiple factors contribute to the undesirable characteristics of PSCs. Among them, ionic motion[10,11] and charge accumulation[6,12–14] at the interfaces have been proposed as a major cause and this can lead to intrinsic degradation of the device. In this context, different strategies have been investigated in order to avoid charge accumulation or ionic motion. Passivation has become one of the best techniques to reduce charge accumulation by improving interfacial contacts[15]. For example, charge collection may be improved by passivating the TiO_2 layer with Al_2O_3[16] and by utilization of the self-passivating nature of tin oxide (SnO_2)[17] in mesoscopic and planar PSCs, respectively. The application of polymers has also been explored in the perovskite precursor solution, which passivates the trap states of the perovskite layer and thus reduces the number of film defects.[18-20]

Ionic liquids (ILs), which are molten salts at room temperature, can passivate interlayer interfaces, favoring better charge extraction, and can also improve device stability by increasing the hydrophobic character to the perovskite film.

Recently, the incorporation of functionalized imidazolium salts was shown to enhance the crystallization process of the perovskite films giving rise to a more efficient and stable PSCs.[21] In addition, functionalization of ILs with a fluorous chain affords perovskite films with a high degree of hydrophobic character.[22,23] Environmental parameters such as humidity, temperature, oxygen and UV light were found to trigger degradation mechanisms in PSCs.[24–27] Surprisingly, light exposure after oxygen inclusion in the structure was found to have a beneficial effect on the stability of perovskite layers.[28] Therefore, an oxazolium-based IL dopant that down-converts UV irradiation could potentially improve the stability of devices providing internal stability with the oxygen ion in its structure. A similar approach using a silane coupling agent that prevents the degradation of the perovskite layer by UV exposure was recently reported.[29]

Here, we describe the synthesis of 2-phenyl-3-methyloxazolium iodide (2Ph-ox) and its incorporation in $MAPbI_3$ based mesoscopic perovskite devices. The electro-optical properties were analyzed in conjugation with its role in determining device performance. Oxazolium salts are air stable, and are class of aromatic cyclic cations which possesses fluorescent properties, additionally their high stability and low diffusivity favors there use as dopants.[30]

Results and Discussion

The 2-phenyl-3-methyloxazolium iodide salt (2Ph-ox), was prepared by the reaction of oxazoline with bromobenzene in the presence of a $Pd(PPh_3)_4$ catalyst, followed by methylation with methyliodide (Scheme 1). The electro-activity of this salt was confirm by recording the cyclic voltammogram which shows higher current density in an aqueous solution.

---

[a] Dr. M. Salado, Dr. S. Kazim and Prof. S. Ahmad*
Basque Center for Materials, Applications and Nanostructures
Bld. Martina Casiano, UPV/EHU Science Park
Barrio Sarriena s/n, 48940 Leioa, Spain Tel: +34 946128811
Email:shahzada.ahmad@bcmaterials.net

[b] IKERBASQUE, Basque Foundation for Science, Bilbao, 48013, Spain

[c] E. Shirzadi, Prof. M. K. Nazeeruddin, Group for Molecular Engineering of Functional Materials, Swiss Federal Institute of Technology Lausanne (EPFL), EPFL Valais Wallis, CH-1951 Sion, Switzerland.

[d] E. Shirzadi, Dr. Z. Fei, Prof. P. J. Dyson, Institute of Chemical Sciences and Engineering, Swiss Federal Institute of Technology Lausanne (EPFL), CH 1015, Lausanne, Switzerland.

10.1002/cplu.201700471

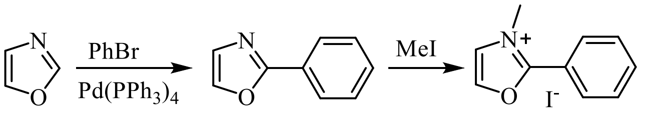

Scheme 1: Synthesis of 2-phenyl-3-methyloxazolium iodide (2Ph-ox).

The absorbance spectrum of 2Ph-ox was recorded in a highly dilute solution (Fig. 1a). The iodide salt 2Ph-ox absorbs intensely in the ultraviolet (UV) region with two main peaks, and showing negligible absorbance in the visible region. The fluorescence emission (Fig. 1b) shows broad emission peak in the visible region. The addition of 2Ph-ox might therefore, not only influence the morphology of the perovskite layer and reduce the pinholes of the perovskite films, but also improve the stability of the devices under ultraviolet irradiation.

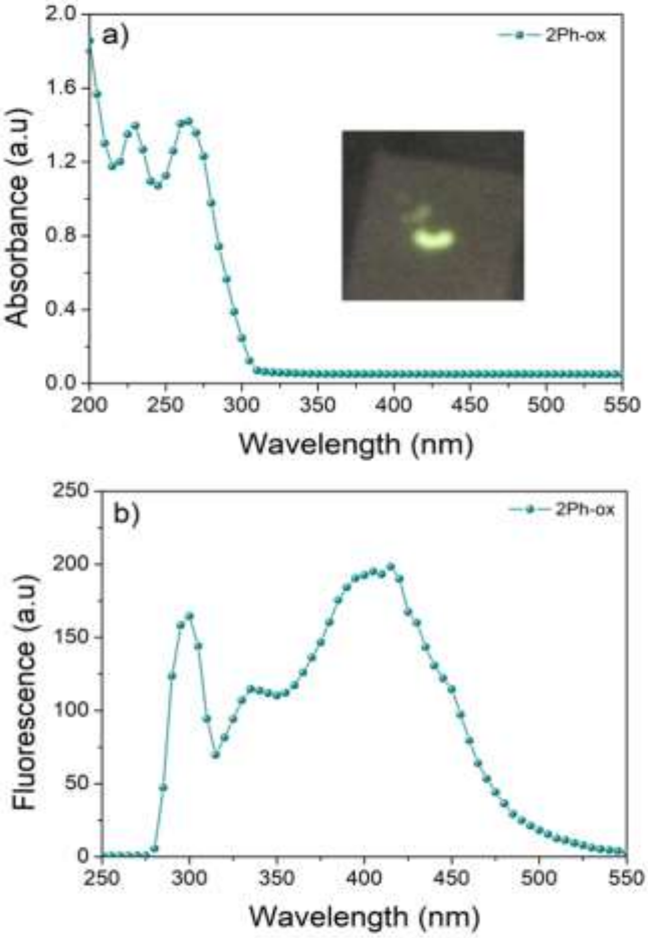

Figure 1. a) Absorption spectrum of 2Ph-ox (0.083 mM), inset shows 2Ph-ox under 365 nm UV illumination and **b**) fluorescence spectrum.

Preparation and characterization of the perovskite films

2Ph-ox was added in varying concentrations as a dopant during the preparation of the $MAPbI_3$ perovskite films with the expectation of passivating the defects. X-ray powder diffraction (XRD) patterns of the doped $MAPbI_3$ perovskite films were recorded under ambient conditions (40-50% RH, Fig. 2). The diffraction patterns of the pure $MAPbI_3$ and 2Ph-ox-doped films are essentially the same. The characteristic peak of PbI_2 at 12.6° is absent (denoted by the red dotted line and asterisk in Fig. 2). This characteristic peak appears when the perovskite layers degrade, and is indicative of a water-based decomposition pathway, and since this peak is not observed such a pathway may be excluded. Consequently, the 2Ph-ox is presumably in an amorphous state or is well dispersed in the films.

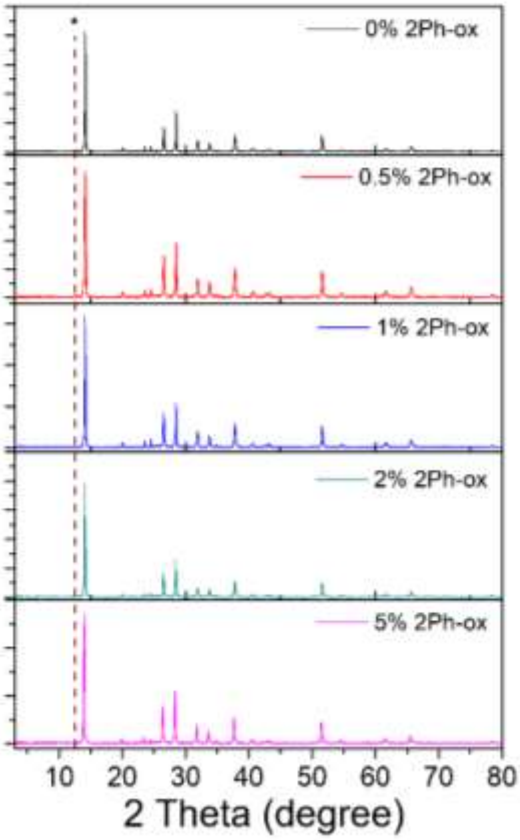

Figure 2. XRD patterns of the perovskite films with different % (w/w) 2Ph-ox. Red dotted line indicates where the characteristic peak of PbI_2 is located (12.6°).

Evaluation of device performance

The absorbance spectra of the perovskite layers doped with 2Ph-ox are shown in Fig. 3a, and reveal that the inclusion of 2Ph-ox in the structure has negligible influence on the perovskite layer absorption in the broad part of the spectrum. No new absorbance band is observed at a loading of 2Ph-ox. Uniform perovskite deposition was observed even, with the inclusion of higher amount of the oxazolium salt, which is on the contrary to previous research where the addition of 5% fluorous imidazolium cation referred as FIm produce a patchy surface.[20] The absorption coefficient (α) was calculated by measuring total transmittance and the Tauc plot method was applied to estimate the direct band gap, i.e. linear extrapolation of the $(\alpha h\nu)^2$ versus $h\nu$ curve, to intercept the horizontal energy axis (Fig. 3b), with no significant change was observed.

10.1002/cplu.201700471

This behavior indicates that although the dopant does not insert inside the crystalline structure, presumably due to its large size exceeding the Goldschmidt limit [25], and the band gap remains largely unchanged. We hypothesize that 2Ph-ox, with a Lewis basic O-atom, can passivate the defects and therefore increase photon-to-electron conversion efficiencies.

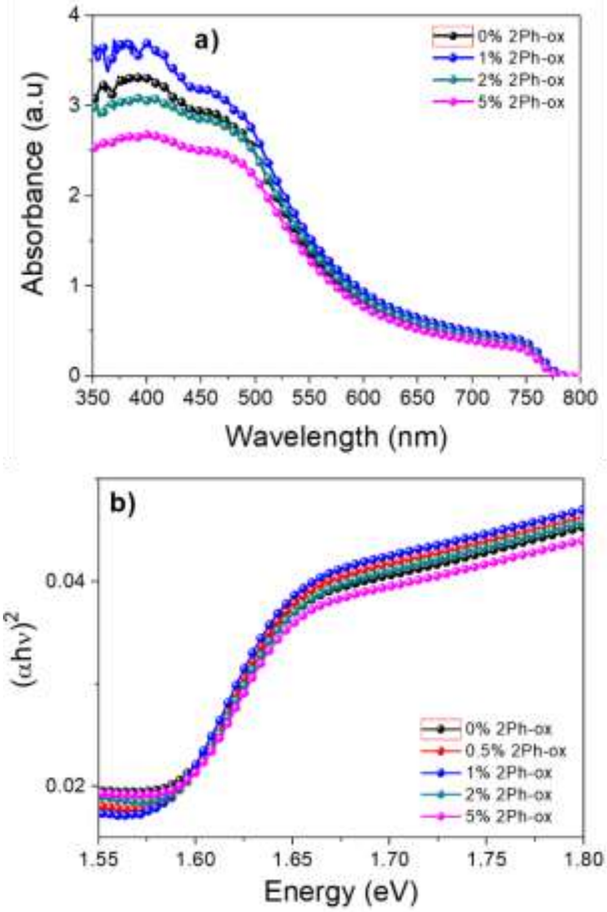

Figure 3. a) The absorption spectra and **b**) the Tauc plot of the pure and Ph-ox doped perovskite films.

Table 1. Photovoltaic parameters and device statistics under 100 mW cm^{-2}.

Doping ratio	V_{oc}(mV)	J_{sc}(mAcm^{-2})	*FF* (%)	*PCE* (%)
0%	1086±9.9	22.73±0.22	76.1±1.9	18.78±0.60
0.5%	1078±10.6	22.89±0.5	76.8±2.9	19.16±0.85
2%	1100±6.9	21.55±0.24	73.0±5.38	17.37±1.40
3.5%	1109±15.3	21.03±0.67	76.0±3.6	17.73±1.24
5%	1121±15.5	18.52±0.33	78.0±2.4	16.19±1.50

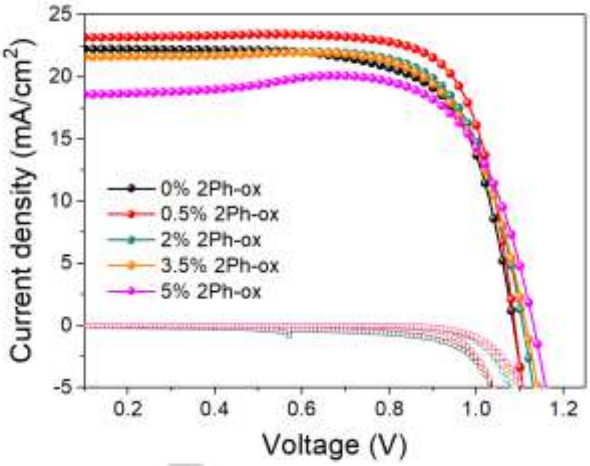

Figure 4. *J–V* characteristics for devices containing perovskite films with different concentrations of the 2Ph-ox dopant under 100 mW cm^{-2} AM1.5G irradiation.

Table 1 and Figure 4 summarize the characteristic photovoltaic parameters of the devices. Notably, with 0.5% of 2Ph-ox the photocurrent and fill factor (*FF*) as well as the power conversion efficiency (*PCE*) are improved, which indicates lower recombination losses or shunting paths into the solar cell devices. As is apparent from Figure 4, loading of perovskite layers with ≥ 2% 2Ph-ox affords a slightly higher open circuit voltage (V_{oc}) compared to pristine or 0.5% 2Ph-ox devices, which may be attributed to either shifting of the Fermi level or lower recombination rates, but at the expense of short circuit current density (J_{SC}). This observation is in accordance with the optical band gap calculation (Fig. 3b). The decrease in short circuit current could be due to lower absorption in the perovskite layers. The best *FF* and J_{SC} was shown by the cell containing the perovskite film with 0.5% of 2Ph-ox, which is also in accordance with our earlier results. Notably, a *FF* up to c.a 76.80% was obtained at this loading (Table 1, entry 2), which we attribute to the formation of uniform perovskite grains as the addition of 2Ph-ox, we assume its inclusion also modifies the crystallization process. However, at high loadings of 2Ph-ox, the short circuit current is affected due to possible charge extraction blocking, as evident in Figure 6 for the device with 5% 2Ph-ox. Higher percentage of 2Ph-Ox will shift the bandgap of $MAPbI_3$, upwards and produce relatively higher open circuit voltage, as a result lower short circuit voltage.

Modification of the perovskites by the addition of 2Ph-ox influences the crystallization rate, crystal size and film microstructure. The improvement in the film quality also entails a reduction of the pinholes, i.e. there are fewer recombination sites, which in turn improves the PV performance. Figures 5a and 5b depict the microstructure of the respective perovskite layers with and without the addition of the 2Ph-ox dopant.

10.1002/cplu.201700471

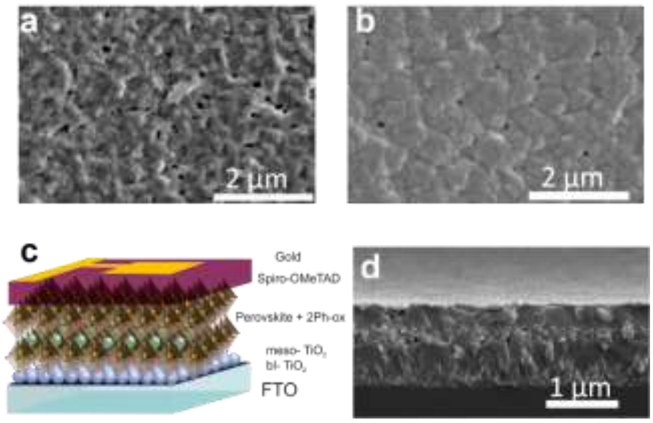

Figure 5. Scanning electron microscopy images of perovskite layers a) without the 2Ph-ox dopant and b) with 4% (w/w) 2Ph-ox, c) Schematic of the fabricated solar cell used in this work and d) cross-sectional image of the fabricated 2Ph-ox doped solar cell.

The addition of 2Ph-ox produces more uniform and larger perovskite crystals, as compared to the pristine perovskite, with a cubic-shape and small crystal size. Figure 5c illustrates the device configuration used and is in accordance with the cross section image of the fabricated device (Figure 5d). Well identified layers, with sharp interfaces are visible (Figure 5d), which confirms the architecture depicted in the schematic in Figure 5c. We assume, oxazolium cation will help to protect the perovskite layers from harmful UV exposure (which degrades the devices) and it will down-convert the radiation to be emitted at higher wavelength.

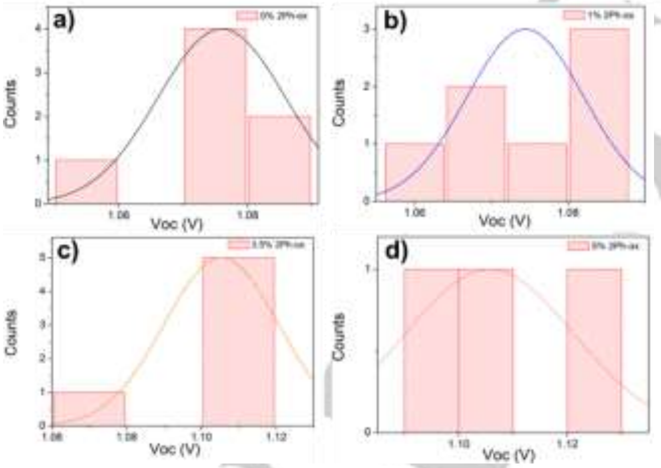

Figure 6. Open circuit voltage (V_{oc}) distribution of devices with different 2Ph-ox loadings.

Figure 7 shows the photon-to-electron conversion efficiencies as a response of wavelength and represented as incident photon-to-current conversion efficiency (IPCE) plots for the various devices. From the graph, the IPCE values in these systems approaches unity (>90%) in the broad range of visible spectrum, except in the case of devices fabricated from perovskites doped with high levels of 2Ph-ox, which yield lower IPCE values. The secondary Y-axis represents the derived integrated current value, which is in accordance with the experimental error bar of the *J-V* measurements.

Relatively flat photon-to-electron conversion profiles were observed between 400 and 750 nm. As expected, devices containing perovskite films doped with 2.5% and 3.5% 2Ph-ox exhibit lower IPCE values, which is in line with device *J-V* properties.

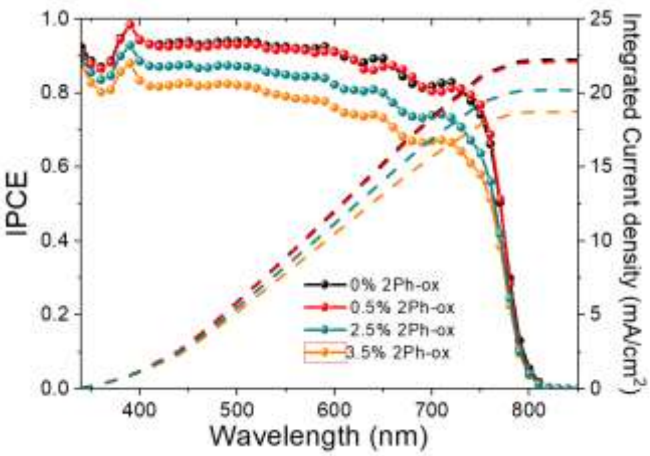

Figure 7. IPCE spectra of the fabricated solar cells under AM1.5G irradiation. Dash line represents integrated current density of devices.

Conclusions

The inclusion of the 2-phenyl-3-methyloxazolium iodide (2Ph-ox) dopant in $MAPbI_3$ based solar cells has been studied as the hydrophobic cation in this salt down-converts UV light into visible light, which could improve both the stability and the efficiency of PSCs. The perovskite microstructure shows signs of improved crystallization in the presence of 2Ph-ox. At low concentrations the 2Ph-ox dopant does not alter device photo-physical properties as well as the kinetics and overall the device photovoltaic parameters are improved. This simple approach is worth further investigation and a wide and diverse range of oxazolium and other salts could be used to tune the parameters of PSCs based on high performance perovskite layers.

Experimental Section

Chemicals were obtained from commercial sources and used without further purification. ^{1}H-NMR and proton-decoupled ^{13}C-NMR spectra were recorded on a Bruker Avance-400 (400 MHz) spectrometer. 2-Phenyloxazole was synthesized using a literature method.[31] Spectroscopic data for the product is in agreement with that previously reported.

Synthesis of 2-phenyl-3-methyloxazolium iodide (2PH-ox): 2-phenyloxazole (200 mg, 1.38 mmol) was dissolved in dry acetonitrile (3 mL) under nitrogen atmosphere, then iodomethane (590 mg, 4.13 mmol) was added dropwise to the solution. The resulting mixture was stirred at 110°C for 48h. After the reaction was complete, the solvent was removed under vacuum and the resulting solid was washed with ethyl acetate (3x 3mL). Afterwards, the solid was dissolved in minimum of acetonitrile and crystalized by dropwise addition of diethyl ether. The white needle like crystals were collected by filtration, dried to give the pure product (240 mg, 61%), ^{1}H NMR (400 MHz, DMSO-d6, δ): 8.86 (d, 1H, Ox H), 8.38 (d, 1H, Ox H),8.07 (m, 2H, Ar-H), 7.78 (m, 1H, Ar-H), 7.77 (m, 2H, Ar-H),4.09 (s, 3H, CH_3); ^{13}C NMR (100 MHz, DMSO-d6, δ): 161.1, 142.6, 134.8, 130.2, 130.02, 126.0, 120.6, 37.5.

Solar cell fabrication

PSCs were fabricated on FTO glass substrates (NSG10), prior to use it was cleaned by ultrasonication using a 2% Hellmanex solution, followed by washing with acetone and isopropanol. To burn any surface moieties, it was then treated with UV ozone for 20 min. The FTO substrates were fired to 500°C and a compact TiO_2 as blocking layer was then deposited by spray pyrolysis, using a diluted (1/19 ml) titanium diisopropoxidebis(acetylacetonate) solution in ethanol and was heated for 30 minutes. The mesoporous layer (30 NRD TiO_2 paste from Dyesol) was deposited by spin-coating of diluted TiO_2 dispersion in ethanol, ratio 1:8 (w/v), at 2000 rpm for 10s followed by annealing at 500°C for 30 min in steps. The photoanode was then treated with lithium bis(trifluoromethylsulfonyl)imide (Li-TFSI) by spin-coating 50 µl onto the mesoporous layer, followed by a sintering step at 500°C for 30 min. All the solution and perovskite layer were deposited inside an argon filled glove box under controlled moisture and oxygen conditions (H_2O level:1 ppm and O_2 level:10 ppm) and kept under stirring at 80°C overnight in order to dissolve completely PbI_2. Stoichiometric precursor solutions (1.25 M) were prepared by mixing MAI (Sigma Aldrich) and PbI_2 (TCI) in dimethylsulfoxide (DMSO). The oxazolium iodide salt 2Ph-ox at different concentration (0.5, 1, 2, 3, 4, and 5 mg/ml) were added as dopant to the perovskite precursors solution. The resulting solution was deposited using a two-steps spin-coating process, first step 1,000 r.p.m. for 10s; second step 3,500 r.p.m for 30 s. During the second step 110 µl of chlorobenzene were used as antisolvent approach and was dropped on substrates 10s prior to the end of the program, the perovskites were annealed at 100°C for 40 min. Once the samples attain room temperature, Spiro-OMeTAD was spun coated at 4000 rpm for 30 s by dissolving 72.3 mg of Spiro-OMeTAD in 1 ml of chlorobenzene; 21.9 mL of tris(2-(1H-pyrazol-1-yl)-4-tert-butylpyrydine) cobalt(III) bis(trifluoromethylsulphonyl) imide (FK209) from stock solution (400 mg of FK209 in 1 ml of acetonitrile), 17.5 mL of lithium bis-(trifluoromethylsulphonyl) imide (LiTFSI) stock solution (520 mg of LiTFSI in 1 ml of acetonitrile) and 28.8 mL of 4-tert-butylpyridine were also added to the solution as dopants. The devices were finished by depositing 70 nm of gold by thermal evaporation, as a cathode layer.

Thin film Characterization

For structural characterization, thin films were prepared by spin coating of $MAPbI_3$ and $MAPbI_3$ + 2Ph-Ox solutions onto glass. X-ray diffractograms were recorded using a D8 Advance diffractometer from Bruker (Bragg-Brentano geometry, with an X-ray tube Cu Kα, λ=1.5406Å). A scan range of 3°–80° was selected with an acquisition time of 1 degree per min. The absorption spectra were registered with an UV-VIS-IR spectrophotometer (PerkinElmer Instrument). The perovskite film morphology was analysed using a FEI Teneo scanning electron microscope (SEM) using an electron beam accelerated at 5 kV.

Device Characterization

Current density–voltage (*J*–*V*) curves were recorded using a VeraSol LED solar simulator (Newport) producing 1 sun AM 1.5 (1000W/m^2) sunlight. *J*–*V* curves were measured in air with a potentiostat (Keithley 2604). The light intensity was calibrated with a NREL certified KG5 filtered Silicon reference diode. *J-V* measurement were performed at 100 mV s^{-1} scan rate (pre sweep delay: 10s) and a black metal mask (0.16 cm^2) was used over the square solar cell active area to reduce the influence of scattered light, without using any anti-reflective coating during the measurement. Incident photon current efficiency (IPCE) measurements were carried out using a 150 W Xenon lamp (Newport) attached to with IQE200B (Oriel) motorized 1/4m mono-chromator as the light source, and no bias light was applied.

Keywords: solar cells • perovskite solar cells • perovskites • ionic liquids • oxazolium salts

[1] W. S. Yang, B.-W. Park, E. H. Jung, N. J. Jeon, Y. C. Kim, D. U. Lee, S. S. Shin, J. Seo, E. K. Kim, J. H. Noh, et al., *Science (80-.).* **2017**, *356*, 1376–1379.

[2] H. S. Jung, N. G. Park, *Small* **2015**, *11*, 10–25.

[3] Y. Yang, J. You, *Nature* **2017**, *544*, 155–156.

[4] H. J. Snaith, A. Abate, J. M. Ball, G. E. Eperon, T. Leijtens, N. K. Noel, S. D. Stranks, J. T. W. Wang, K. Wojciechowski, W. Zhang, *J. Phys. Chem. Lett.* **2014**, *5*, 1511–1515.

[5] E. L. Unger, E. T. Hoke, C. D. Bailie, W. H. Nguyen, A. R. Bowring, T. Heumüller, M. G. Christoforo, M. D. McGehee, *Energy Environ. Sci.* **2014**, *7*, 3690–3698.

[6] C. Zhao, B. Chen, X. Qiao, L. Luan, K. Lu, B. Hu, *Adv. Energy Mater.* **2015**, *5*, DOI 10.1002/aenm.201500279.

[7] V. Gonzalez-Pedro, E. J. Juarez-Perez, W. S. Arsyad, E. M. Barea, F. Fabregat-Santiago, I. Mora-Sero, J. Bisquert, *Nano Lett.* **2014**, *14*, 888–893.

[8] H. S. Kim, N. G. Park, *J. Phys. Chem. Lett.* **2014**, *5*, 2927–2934.

[9] H.-S. Kim, I.-H. Jang, N. Ahn, M. Choi, A. Guerrero, J. Bisquert, N.-G. Park, *J. Phys. Chem. Lett.* **2015**, acs.jpclett.5b02273.

[10] C. Eames, J. M. Frost, P. R. F. Barnes, B. C. O'Regan, A. Walsh, M. S. Islam, *Nat. Commun.* **2015**, *6*, 7497.

[11] J. M. Azpiroz, E. Mosconi, J. Bisquert, F. De Angelis, *Energy Environ. Sci.* **2015**, *8*, 2118–2127.

[12] H.-S. Kim, I. Mora-Sero, V. Gonzalez-Pedro, F. Fabregat-Santiago, E. J. Juarez-Perez, N.-G. Park, J. Bisquert, *Nat. Commun.* **2013**, *4*, 2242.

[13] B. Wu, K. Fu, N. Yantara, G. Xing, S. Sun, T. C. Sum, N. Mathews, *Adv. Energy Mater.* **2015**, *5*, DOI 10.1002/aenm.201500829.

[14] I. Zarazua, J. Bisquert, G. Garcia-Belmonte, *J. Phys. Chem. Lett.* **2016**, *7*, 525–528.

[15] T. Zhang, N. Guo, G. Li, X. Qian, Y. Zhao, *Nano Energy* **2016**, *26*, 50–56.

[16] Y. H. Lee, J. Luo, M. K. Son, P. Gao, K. T. Cho, J. Seo, S. M. Zakeeruddin, M. Grätzel, M. K. Nazeeruddin, *Adv. Mater.* **2016**, *28*, 3966–3972.

[17] Y. H. Lee, S. Paek, K. T. Cho, E. Oveisi, P. Gao, S.-H. Lee, J.-S. Park, Y. Zhang, R. Humphry-Baker, A. M. Asiri, et al., *J. Mater. Chem. A* **2017**, *28*, 3966–3972.

[18] T. Zhang, L. Xie, L. Chen, N. Guo, G. Li, Z. Tian, B. Mao, Y. Zhao, *Adv. Funct. Mater.* **2016**, *27*, 1603568.

[19] K.-G. Lim, H.-B. Kim, J. Jeong, H. Kim, J. Y. Kim, T.-W. Lee, *Adv. Mater.* **2014**, *26*, 6461–6466.

[20] C.-C. Zhang, M. Li, Z.-K. Wang, Y.-R. Jiang, H.-R. Liu, Y.-G. Yang, X.-Y. Gao, H. Ma, *J. Mater. Chem. A* **2017**, *5*, 2572–2579.

[21] Y. Zhang, Z. Fei, P. Gao, Y. Lee, F. F. Tirani, R. Scopelliti, Y. Feng, P. J. Dyson, M. K. Nazeeruddin, *Adv. Mater.* **2017**, *29*, 1702157, DOI 10.1002/adma.201702157.

[22] M. Salado, M. A. Fernández, J. P. Holgado, S. Kazim, M. K. Nazeeruddin, P. J. Dyson, S. Ahmad, *ChemSusChem* **2017**, *10*, 3846-3853.

[23] M. Salado, F. J. Ramos, V. M. Manzanares, P. Gao, M. K. Nazeeruddin, P. J. Dyson, S. Ahmad, *ChemSusChem* **2016**, *9*, 2708–2714.

[24] T. A. Berhe, W.-N. Su, C.-H. Chen, C.-J. Pan, J.-H. Cheng, H.-M. Chen, M.-C. Tsai, L.-Y. Chen, A. A. Dubale, B.-J. Hwang, *Energy Environ. Sci.* **2016**, *9*, 323–356.

[25] A. Guerrero, J. You, C. Aranda, Y. S. Kang, G. Garcia-Belmonte, H. Zhou, J. Bisquert, Y. Yang, *ACS Nano* **2016**, *10*, 218–224.

[26] R. K. Misra, S. Aharon, B. Li, D. Mogilyansky, I. Visoly-Fisher, L. Etgar, E. A. Katz, *J. Phys. Chem. Lett.* **2015**, *6*, 326–330.

[27] D. Wang, M. Wright, N. K. Elumalai, A. Uddin, *Sol. Energy Mater. Sol. Cells* **2016**, *147*, 255–275.

[28] R. Brenes, D. Guo, A. Osherov, N. K. Noel, C. Eames, E. M. Hutter, S. K. Pathak, F. Niroui, R. H. Friend, M. S. Islam, et al., *Joule* **2017**, *1*, 155–167.

[29] Y. Sun, X. Fang, Z. Ma, L. Xu, Y. Lu, Q. Yu, N. Yuan, J. Ding, *J. Mater. Chem. C* **2017**, *5*, 8682-8687.

[30] Z. Bin, L. Duan, Y. Qiu, *ACS Appl. Mater. Interfaces* **2015**, *7*, 6444–6450.

[31] F. Besselièvre, S. Lebrequier, F. Mahuteau-Betzer, S. Piguel, *Synthesis.* **2009**, 3511–3518.

Entry for the Table of Contents

Layout 1:

ARTICLE

Employment of oxazolium cation to protect the light harvesting perovskite layer from environmental exposure.

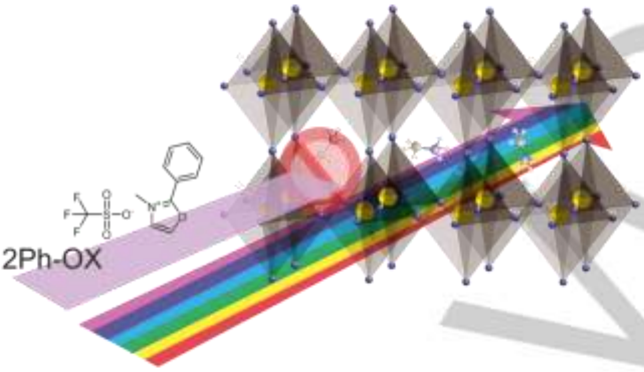

*Manuel Salado, Erfan Shirzadi, Samrana Kazim, Zhaofu Fei, Mohammad Khaja Nazeeruddin, Paul J. Dyson, Shahzada Ahmad**

Page No. – Page No.

Title